Desalination and Water Treatment
www.deswater.com
doi: 10.5004/dwt.2021.27344

228 (2021) 47–62
July

Design and economic assessment of an autonomous flexible wind energy system powering a large capacity water desalination plant

Emad Ali[a,*], Mourad Bumazza[a], Ali Eltamaly[b,c], Sarwono Mulyono[a], Muath Yasin[a]

[a]*Chemical Engineering Department, King Saud University, Riyadh 11421, Saudi Arabia, emails: amkamal@ksu.edu.sa (E. Ali), mouradb@ksu.edu.sa (M. Bumazza), sarmulyoprayitno@ksu.edu.sa (S. Mulyono), 439105965@student.ksu.edu.sa (M. Yasin)*
[b]*Sustainable Energy Technologies Center, King Saud University, Riyadh 11421, Saudi Arabia, email: eltamaly@ksu.edu.sa*
[c]*Electrical Engineering Department, Mansoura University, Mansoura, Egypt*

Received 4 October 2020; Accepted 20 April 2021

ABSTRACT

In this study, we present a novel methodology to design and optimally operate a standalone wind-driven reverse osmosis desalination plant to provide the required water production in face of fluctuating wind power. The methodology is applied to a plant with a capacity of 2,592 m^3/h for a rural area in Saudi Arabia. The plant nominal size, operating conditions, and the number of wind turbines are determined through numerical simulations. The performance of the desalination plant is tested under fluctuating wind power using two different operation strategies that allow for better leverage of the generated wind power. It is found that the desalination system can provide the annual production capacity if the feed pressure is optimally adapted in response to the varying wind speed. Another successful strategy involves the optimal use of the plant vessels in face of fluctuating wind power. Both strategies are successful but necessitate the use of a control system to automatically adapt the feed pressure or the plant active vessels during wind power variations. Moreover, the economic analysis signified a water cost as low as 0.45 \$/m^3 for the studied plant.

Keywords: Desalination; Reverse osmosis; Wind power; Water cost; Adaptive design

1. Introduction

Desalination of brackish water [1] and seawater [2] is a technology that is used in several countries to satisfy water demand. However, the common challenges facing water desalination technologies are high-energy consumption and adverse effects on the environment. Reverse osmosis (RO) is believed to call for the least energy demand among existing desalination technologies [3]. The major portion of the consumed energy is related to pressurizing feed water. Yet, the cost of electric energy is vulnerable to fossil fuel prices. It was reported that 25% fluctuations in energy cost can cause 11% variations in the specific water cost [4]. To avoid such cost fluctuations, integrating RO desalination systems with solar or wind energy is becoming an attractive alternative that calls for growing attention.

Saudi Arabia is an arid country with an increasing demand for freshwater and electricity. Due to the vast area of the country, several satellite stations and remote regions need an independent source of power as well as potable water. Thereby, the kingdom has established a long-term plan to increase its reliance on renewable energy resources. According to the nation 2030 vision, 40 GW of solar energy, and 17 GW of wind energy are targeted to subsidize the oil-based energy source [5]. In fact, according to the latest survey, the kingdom has a viable potential for wind energy resources as the wind speed can be over 3.5 m/s in several areas [5]. Hence it is of potential to harness the available

* Corresponding author.

wind energy in these isolated regions to produce potable water from local aquifers via RO desalination.

Globally, the utilization of wind energy to power RO units has been extensively studied, with more efforts focusing on the reliability of wind-driven RO desalination plants during wind intermittent [6–12]. However, it can be stated that not too much work has been reported to examine the performance of the RO desalination system for brackish water using wind power as the only source of energy. Most studies focused on subsidizing intermittent wind power by hybridization of solar and wind energies or incorporating energy storage devices. Unfortunately, both solutions are costly and complicated as they incur additional instrumentations, power management systems, and automatic control elements. In addition, most of these studies developed a rigid system with fixed component sizing based on a specific operating condition. During realistic operation, these well-designed systems may not perform as ought to be due to unforeseen disturbances other than wind intermittency.

Several studies focusing on the incorporation of wind power to drive RO desalination plants have been conducted [13,14]. These efforts differ on the way to deal with the fluctuation and intermittency of wind energy. Lai et al. [7] outlined different policies to mitigate the harmful influence of heavily variable wind energy on the operation of RO desalination plants. They classified the solutions into three main approaches: using a battery, using hybrid renewable energy resources (RES), and manipulating the system operating conditions. For example, Carta et al. [10] and Richards et al. [15] proposed using a supercapacitor energy bank to subsidize load intermittency due to real wind fluctuations applied to a brackish and seawater RO system. Several authors [16–19] studied the use of hybrid solar and wind energy sources promoted with energy buffering to operate the RO desalination plant. The process can operate smoothly by implementing a power management protocol. Other investigators proposed using automatic control systems and or state-of-the-art intelligent systems to offset the power losses during discontinuity of wind energy [20,21] applied for the operation of a seawater RO plant. In summary, wind speed fluctuation causes challenges in designing and operating the RO system smoothly. Coupling RO plant with solar or wind energy requires additional devices such as battery and power management systems. The coupled RES systems are even more complex because they incur extra instrumentation and control elements [19]. Furthermore, hybrid systems are more expensive as the capital cost of photovoltaic panels is relatively higher [18].

This paper presents a novel scheme for designing stand-alone RO desalination plants to satisfy hourly water demand. The intended scheme helps to select the proper number of wind turbines and RO vessels, as well as the optimal operating mode that produces the required water demand within the available wind power alone. The novelty of this study is thus achieving the aforementioned goal with a proper adaptation of the feed pressure and/or a number of active RO vessels. To our knowledge, no similar procedure has been reported before. Furthermore, this proposed procedure provides flexibility during operation under unexpected disturbances. Another objective of this paper is to assess the economic feasibility of the proposed scheme.

2. RO modeling and simulation

The RO model used in this paper is based on the steady-state model developed by Ali et al. [6] which was derived from previous work [8,9]. The RO model is shown in Appendix A. Table 1 shows the RO membrane specifications [22] used here. The steady-state RO model comprises a set of nonlinear algebraic equations. To solve such a model, the degrees of freedom must be zero which incurs the specification of certain input parameters. The feed salinity, C_f is set equal to the measured salinity of the local brackish water. For the selected city, the local brackish water salinity is around 1.0 kg/m^3 [23]. Accordingly, additional three process variables must be defined to fully solve the RO model. The model will be solved for two important modes: backward and forward modes. In the backward mode, the recovery ratio, R_c, the production rate, Q_p, and the permeate salinity C_p are fixed and are used to solve for the feed pressure, feed flow rate, and the associated power. This backward mode (design mode) will be utilized initially to design the plant size, that is, determining the number of RO vessels and the number of wind turbines.

In the forward mode, the available wind power, P_w, the desired recovery ratio R_c, and the permeate salinity, C_p are fixed and are used to determine the necessary feed pressure, feed flow rate, and production rate. This forward mode (operation mode) will be used to test the plant operation under wind speed variations.

2.1. Backward mode

The required water production of the RO plant can be fixed by the city water consumption. Hence, for a given production rate, the feed pressure, feed flow rate, and the required power per vessel should be determined. These parameters will be calculated by an iterative procedure to meet a specific production rate and predefined permeate quality, that is, the permeate salinity, C_p. The backward mode is described by the optimization algorithm (denoted S1) and shown in Appendix B. Note that the required number of vessels (N_v) is chosen arbitrarily. Because N_v is an integer variable, it will be determined by a grid search to optimize the specific electric consumption (SEC) and to satisfy safe operating conditions as will be discussed later. The total required wind power (P_{wt}) for the desalination plant is thus the necessary power per vessel multiplied by

Table 1
Geometric specification of membrane module [22]

Parameter	Value
Hydraulic diameter of channel, d_h (mm)	0.78045
Height of spacer channel, h_{sp} (mm)	0.593
Void fraction of the spacer, ε (porosity)	0.9
Length of membrane, L (m)	1
Width of membrane, W (m)	37
Active area of the membrane, A_e (m^2)	37
Reference water permeability, A_0 (m^3/h bar)	19.43×10^{-4}
Reference solute permeability, B_0 (m^3/h)	78.55×10^{-5}

the total number of vessels (N_v). Therefore, the total number of required wind turbines (N_{WT}) is simply the total required wind power divided by the rated power of a single turbine.

2.2. Forward mode

In the operation stage, that is, testing the plant operation under available wind power, the forward solution method will be utilized. In this case, the inlet power is given from which the production rate will be determined. The forward mode can be operated into two schemes: variable and fixed pressure. Usually, the RO system should be operated at fixed feed pressures using the nominal value obtained in the design stage (backward model). Nevertheless, in this study, we also examine operating the system using variable pressure which can be regulated by a control system. The optimization algorithm for fixed and variable feed pressure is denoted by (S2) and (S3) and is given in Appendices C and D.

When dealing with renewable energy resources, the reliability of supplying enough power to meet the desired load of the plant is assessed using the loss of power supply probability [24]. Here we adopted the same philosophy to calculate the loss of production probability (LPRP). LPRP will be used to compare the proposed strategies used in the study to withstand wind power intermittency. The loss of production probability is defined as follows:

$$\mathrm{LPRP} = \frac{\sum_{t=1}^{T} Q_P(t) - Q_W(t)}{\sum_{t=1}^{T} Q_P(t)} \tag{1}$$

where T is 1 y in this study which is equivalent to 8,760 h. Note that a value of 1 for LPRP means the required water demand is never satisfied, 0 values denotes satisfaction of the demand, and negative values indicate a surplus of water beyond the needed demand. Hence the goal here is to meet the water demand over the whole year instead of maintaining it at each instant. This means the operation of the RO plant will not be forced to produce the exact hourly demand but to satisfy the annual production demand. But this should not be confused with the ultimate goal that is to supply the required hourly demand to the municipal sector via redistribution of the overall production.

It should be noted that the optimization problem (S1, Appendix B) is used exclusively to optimize the feed pressure of the RO unit to meet the desired production and permeate the quality of the individual RO vessels. This approach resembles the online hourly adaptation of the feed pressure to absorbs the power variation due to wind speed intermittency. Hence, numerical optimization of N_v and/or N_{WT} is not considered here. Rather they will be determined by grid search because they are integer variables. The details of pressure adaptation and determination of N_v and N_{WT} will be discussed in the following sections.

3. Wind-driven RO plant design methodology

The objective here is to design the RO plant configuration necessary to supply the region with the daily water demand via redistributing the accumulated annual production. Fig. 1 presents a topology for the RO plant structure. Several parallel RO vessels, each of which comprise 8 RO elements with 3 leaves [25,26] for each one will be used. Usually, the maximum feed flow rate to a single RO module is limited to avoid damage to the membrane sheet. The ultimate feed flow rate is taken as 15 m^3/h [27]. In addition, a lower limit on the brine flow rate is imposed at 2 m^3/h [27]. For a recovery ratio of 0.75 (maximum value), this limit can be transformed into the feed flow rate to be 2 m^3/h. Consequently, the needed pump capacity is limited by this operational constraint. Accordingly, and because of other constraints, a single RO vessel may not satisfy the necessary water demand of the city. Therefore, a minimum number of RO vessels (N_v) is needed to produce the required water demand. The total required power of the RO plant is thus the product of N_v by the required pump power per vessel, assuming all vessels are identical and operating at the same input conditions. Depending on the available wind speed, a single wind turbine may not be able to supply the total required power. Therefore, several

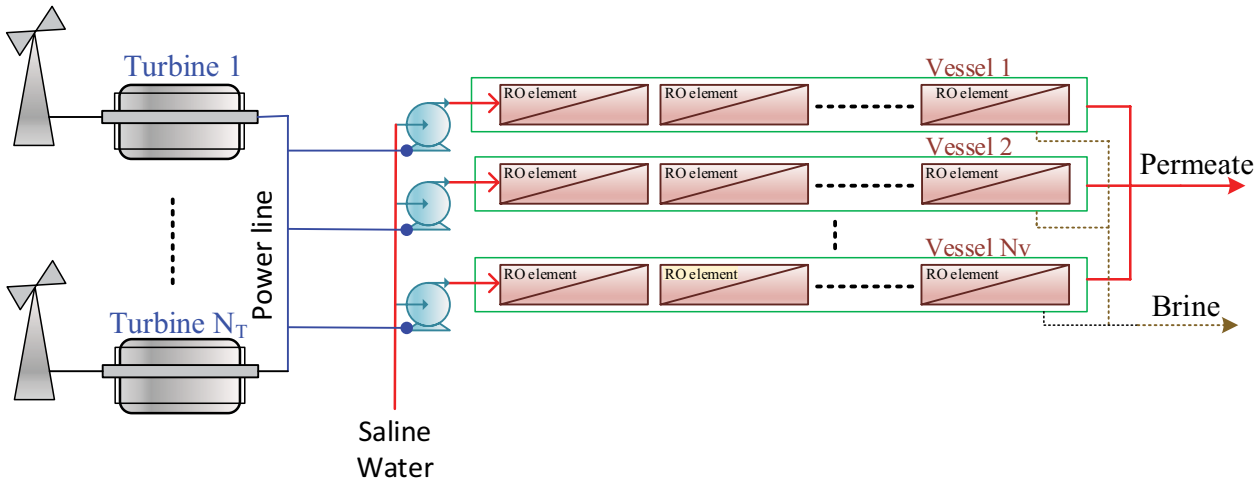

Fig. 1. Wind-driven RO plant structure.

wind turbines are needed as shown in Fig. 1. The selection of the total number of vessels and the operating condition for each vessel will be presented next. Note that determining the number of vessels is not straightforward because water production per vessel is not known in advance as it depends on the necessary feed pressure. Thus, the determination of N_v will be discussed in the next section. Knowing the population of the city in 2020 can reach 311,070 [28] and assuming the daily water consumption per capita is 200 L/d, the hourly water demand of the city is projected to be 2,592 m^3/h. To determine the number of vessels that produce the water demand of 2,592 m^3/h, a grid search will be adopted. The minimum required N_v is tied to the maximum allowable feed flow rate because of $Q_f = 2{,}592/N_v/R_c$. Therefore, for Q_{fmax} = 15 m^3/h and the range of R_c lies between 0.35 and 0.85, the minimum total vessels range between 497 and 230, respectively. Hence, for a given value for N_v and hence $Q_{pv} = 2{,}592/N_v$, the algorithm S1 is solved repeatedly for different values for R_c and N_v. The result is shown in Fig. 2. Figs. 2a–c shows the effect of the recovery ratio on various operating parameters. Particularly, Fig. 2a illustrates the effect of the recovery ratio on the required feed pressure for any N_v value. It can be seen that this pressure increases with the designated recovery ratio which is expected. The feed flow rate on the other hand decreases with the recovery ratio for any value for N_v as shown in Fig. 2b. This also intuitive because as R_c increases, the required feed flow rate for a fixed production will decrease.

For the backward mode, the feed flow rate is independent of the feed pressure, and is calculated directly for the required production rate and desired recovery ratio. Note that for N_v equal 400, the required feed flow rate exceeds the upper limit at very low R_c. This behavior is expected because as mentioned before, the minimum N_v at R_c = 0.35 is 497. This violation may get extended to higher R_c for N_v less than 400. That is why the results for low values of N_v are excluded. Nevertheless, since P_f increases and Q_f decreases with R_c, the pump power per vessel given goes through a minimum. Likewise, the total power, which is proportional to the pump power per vessel, passes through a minimum as depicted in Fig. 2c. However, as the pressure starts growing rapidly, the required power rises as well despite the reduction in the feed flow rate. Similarly, the SEC which is proportional to P_{wt} will certainly exhibit an analogous trend as illustrated in Fig. 2d. It can be concluded that for safe operation over the entire expected recovery ratio, the value of N_v must be at least 500. Using N_v less than 500 will cause the pump to work at the maximum allowable flow rate and hence the extra available wind power will be wasted. Moreover, to minimize the total required power as well as SEC, the RO module should operate at R_c equal to 0.5. Note that increasing N_v will further reduce SEC and P_{wt}. However, this is not recommended because it will increase the capital cost of the RO vessels. Besides, the reduction rate in SEC and P_{wt} becomes smaller as N_v departs way from 500. Therefore, at R_c = 0.5 and N_v = 500, the nominal operating pressure is 7.5 bar, the nominal feed flow rate is 10.4 m^3/h and the required total power is 1,787 kW. The corresponding SEC is 0.69 which is within the reported values in the literature for brackish water [29,30]. Note this is the nominal power requirement for producing 2,592 m^3/h of freshwater, however, the RO plant can operate at a higher supplied load as each RO pump has a maximum capacity of 55.5 kW. The latter is based on the maximum delivered flow rate and pressure of 15 m^3/h and 40 bar, respectively.

4. Design of wind energy system

As has been shown in the previous section, it is required to generate 1,787 kW average power to produce an adequate quantity of water for the city. The design of the energy system starts with studying the wind speed variations in the city. The monthly maximum and mean wind speed in the city are shown in Table 2 [31]. Wind speed in this

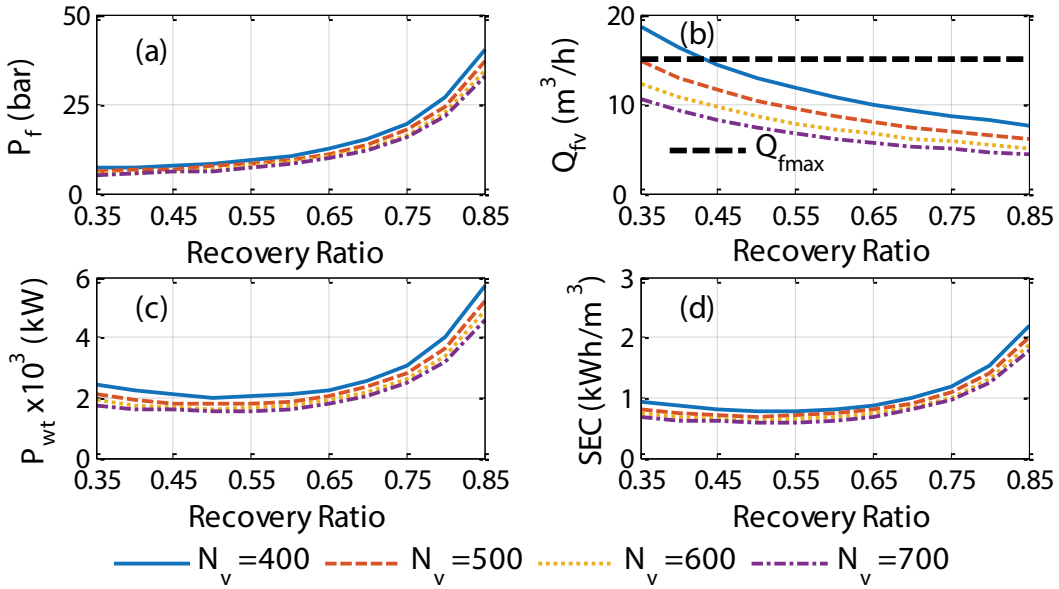

Fig. 2. RO plant performance under different operating conditions.

Table 2
Wind speed for the city on 40 m height [31]

Month	Jan.	Feb.	March	April	May	June	July	Aug.	Sep.	Oct.	Nov.	Dec.	Average
Maximum	16.4	15.2	19.2	18.6	20.7	14.6	15	12.5	18.2	16.5	16.2	20.1	20.7
Mean	5.6	5.5	6.5	6.1	5.9	6.3	6.8	5.7	5.4	5.5	4.9	5.4	5.8

table and Fig. 3 should be determined at the hub height of each wind turbine. The vertical wind speed gradient can be obtained from the following equation [32]:

$$u_w(h) = u_w(h_g)\left(\frac{h}{h_g}\right)^{\alpha} \tag{2}$$

where (h) is the height above the ground level, (h_g) the height of where the wind speed is measured, and (α) is the power-law exponent, which depends on the roughness of the ground surface. Its average value is (1/7) [33].

The wind speed u_w is distributed as the Weibull distribution if its probability density function can be expressed by the following equation:

$$f(u_w) = \frac{k}{c}\left(\frac{u_w}{c}\right)^{k-1}\exp\left(-\left(\frac{u}{c}\right)^{k}\right),\ (k>0, u_w>0, c>1) \tag{3}$$

This is a two parameters distribution where c and k are the scale parameter and the shape parameter, respectively. Curves $f(u_w)$ are given in Fig. 3, for the scale parameter $c = 1$.

The value of c and k can be determined from the iterative process described in [34] and shown in the following equation:

$$k = \left(\frac{\sum_{i=1}^{N} u_i^k \ln(u_i)}{\sum_{i=1}^{N} u_i^k} - \frac{\sum_{i=1}^{N}\ln(u_i)}{N}\right)^{-1} \tag{4}$$

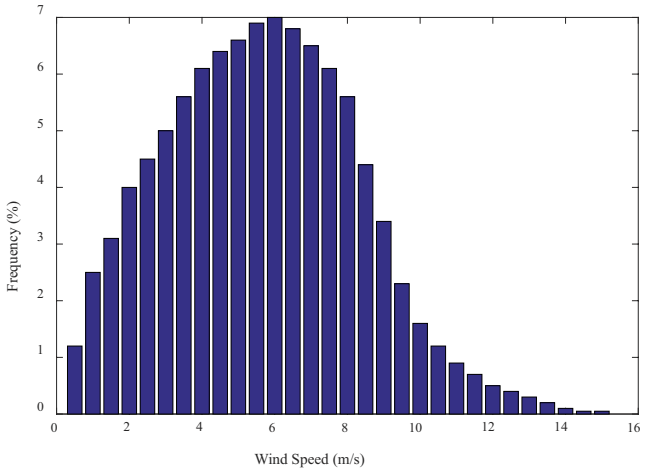

Fig. 3. Wind speed distribution of the site.

where u_i is the wind speed in time step i and N is the number of time steps. Once the shape parameter k has been determined, the following equation could be used to calculate the value of scale parameter c:

$$c = \left(\frac{\sum_{i=1}^{N} u_i^k}{N}\right)^{\frac{1}{k}} \tag{5}$$

These values of scale and shape parameters will be used to determine the capacity factor from the following equation:

$$C_F = \frac{\exp\left[-(u_c/c)^k - \exp\left[-(u_r/c)^k\right]\right]}{(u_r/c)^k - (u_c/c)^k} - \exp\left[-(u_F/c)^k\right] \tag{6}$$

$$P_{w,\mathrm{av}} = C_F P_r \tag{7}$$

The required average number of wind turbines (ANWT) is given by the following equation:

$$\mathrm{ANWT} = \frac{P_{\mathrm{LW,av}}}{P_{W,\mathrm{av}}} \tag{8}$$

where (P_r) is the rated power of wind turbines, ($P_{\mathrm{LW,av}}$) is the average required load, and ($P_{W,\mathrm{av}}$) is the average electric power generated from each wind turbine.

The hourly generated power from the wind turbine is [32]:

$$P_w(u) = \begin{cases} 0 & u \le u_c \ \&\ u \ge u_F \\ P_r\dfrac{u^k - u_c^k}{u_r^k - u_c^k} & u_c \le u \le u_r \\ P_r & u_r \le u \le u_F \end{cases} \tag{9}$$

where P_r is the wind turbine rated power, u is the wind speed and u_c, u_r, u_F are the wind turbine cut-in, rated, and cut-off speeds, respectively.

A total of ten types of wind turbines were examined. The data for each wind turbine is shown in Table 3. It is clear from this table that the highest capacity factor is associated with the AE-Italia wind turbine and for this reason, it will be used in the simulation of the coming parts. Ninety AE turbines will be used to provide an average power of 1,787 kW which covers the required power of the RO plant to supply the necessary water demand. Note that the rated power for 90 turbines is 5,400 kW at the rated wind speed of 8 m/s.

Table 3
Wind turbines data, capacity factor and number of wind turbines in the site

Name	Rated power (kW)	Height (m)	u_c (m/s)	u_r (m/s)	u_f (m/s)	C (m/s)	K	C_F	N_{WT}
ADES ADES 60 [41]	60	27	3.5	8	20	5.4830	2.5649	0.2834	105
Hummer H25 [42]	100	50	2.5	10	20	5.9875	2.5649	0.2417	74
Aeolos-H [43]	100	36	3	10	25	5.7130	2.5649	0.2021	89
Norvento nED [44]	100	40	3	10	20	5.7997	2.5649	0.2109	85
AIRCON 10S [45]	100	40	2.5	10	25	5.7997	2.5649	0.2223	80
AWD-D2CF [46]	200	40	3	10.9	20	5.7997	2.5649	0.1698	53
AIR 19 [47]	100	45	3.5	14	24	5.8981	2.5649	0.0862	207
Allgaier StGW-34 [48]	100	23	3.7	9.5	25	5.3588	2.5649	0.1684	106
AE-Italia [49]	60	30	2.5	8	25	5.5661	2.5649	0.3325	90
Dencon Tornado [50]	200	32	3	12	25	5.6177	2.5649	0.1202	75

The designed water desalination system is tested using the chosen wind turbines and the existing hourly wind speed of the city site. The numerical analysis is performed without using a battery storage system or interconnection with the utility grid. This analysis is achieved by using the algorithm (S2, Appendix C).

4.1. Stand-alone wind energy system without battery

In this system, the load will be connected directly to the wind energy system without battery or interconnection with the electric utility. In this case, the load will able to get more energy than the RO needed value of 1,787 kW when there is higher generated power from the wind turbine. Whereas, if the generation is lower than the needed load (1,787 kW) the RO system will work at its partial capacity and will not have the ability to produce the full required production. Fig. 4 shows the hourly generated power over 1 y based on the hourly wind speed of the city using ninety turbines. The wind speed in Fig. 4a is taken from Bawah et al. [35]. Note the turbine will not generate power higher than the rated value when the wind speed exceeds 8 m/s. The surplus power is the power that equals and exceeds the target value of 1,787 kW, while the deficit power is that below the target value. Thereby according to Fig. 4, the power surplus is 77% and the deficit is 23%. The system in this case will work 4,405 h with partial capacity and the deficit in energy is 23%. Out of the 77% surplus, the system will lose 46% of the total energy generated because there is no way to store this amount of energy. Since the surplus power is more than 3 folds the deficit power, there are two ways to utilize the excess wind power. One way is to utilize the excess power to generate surplus distillate water to offset the water deficit that occurs when the wind power is less than the target value. The second way is to store the excess power in batteries to be used whenever a shortage of

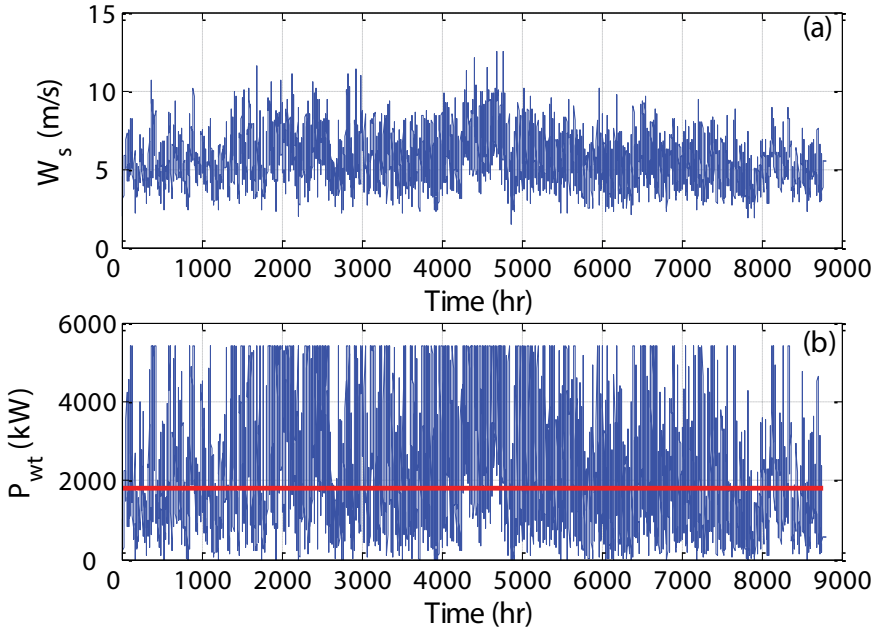

Fig. 4. Annual wind properties profile for the site (a) wind speed and (b) generated power; constant line denotes the target value.

wind power prevails. Hence, sufficient energy is available to run the RO plant throughout the year without a deficit.

5. RO system operation under variable wind energy

5.1. Fixed feed pressure

We will consider the first method using the proposition that the total available wind power is distributed evenly over the total number of vessels. If the relationship between the power and RO production is linear, then one can affirm that the existing wind power is enough to produce the amount of pure water that covers and exceeds the annual demand of the city. This is based on the proposition that the excess water produced during high wind periods can be stored to balance the water shortage during the low wind period. However, the relationship is nonlinear. Moreover, it is not recommended to operate the RO plant under excessive fluctuations in supplied power because it impairs the pumps, instrumentations, and membrane sheets. Nevertheless, we simulate the RO plant using the wind power shown in Fig. 4b to study these situations. This means that we simulate the RO plant using algorithm S3 (Appendix D) at P_f of 7.5 bar. It should be noted when the feed pressure is fixed, the recovery ratio will no longer be fixed, that is, it varies with inlet power. The result is shown in Figs. 5 and 6 when the lower and upper bounds are not imposed on the feed flow rate in the numerical simulation. Ignoring the physical limits is impractical but is shown here for demonstration purposes. Fig. 5d illustrates how the desired water purity is met over the entire timespan. Fig. 5b shows how the feed flow rate per vessel fluctuates with wind power exceeding the physical limits. The generated total production rate is shown in Fig. 5c which illustrates how it fluctuates around the desired production. In this case, the percent surplus in water production amounts to 68% and the percent deficit sums up to 32%. Therefore, the overall balance indicates that the water surplus may compensate for the losses. Moreover, in each region, the production varies in magnitude. Hence, the sum of each region does not necessarily match their corresponding percentages. For this reason, a better comparison of the production with the target value is demonstrated by drawing their accumulative values with time as shown in Fig. 5a. The trend shows a good agreement, but to exactly assess the comparison we compute the loss of production probability which amounts to 0.128 which means there is a 13% shortage in production over a year. For better visualization of the feed and production flow rates, they were redrawn vs. the wind power as depicted in Fig. 6. In this drawing, the wind power is sorted ascendingly and the flow rate correspondingly. It is clear that the feed flow rate propagates proportionally with wind power because the feed pressure is kept constant as shown in Fig. 5a. The feed flow rate obviously violates the physical limits because the limits were not enforced as mentioned earlier. The corresponding production rate increases with feed flow rate/wind power but nonlinearly because it is constrained by the underlying physics of the RO process. At low wind power, that is, less than 500 kW, the production rate is zero because the corresponding feed flow rate is less than the lower limit of 2.5 m^3/h. Note that we did not impose a limit on the feed flow rate, but we choose not to run the RO process when the flow rate is lower than the operational limit. Nevertheless, the result of Figs. 5 and 6 is shown for analysis but it will not be considered because it is not practical.

Next, we re-simulate the RO system while enforcing the physical limit on the feed flow rate. The results are shown

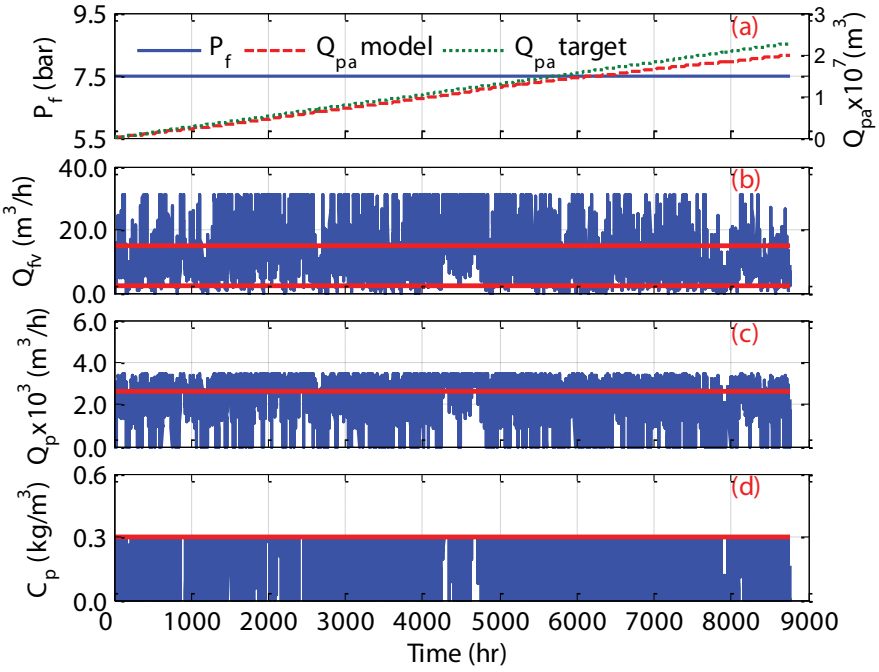

Fig. 5. Simulation of the RO plant at fixed P_f without constraints on the feed flow rate; constant bold line denotes target value for C_p and Q_p and upper and lower limits for Q_f.

in Figs. 7 and 8. In this case, the feed flow rate is contained within the limits as shown in Fig. 7b. It is worth to be noted that, the lower limit is not violated but the feed flow rate is set to equal zero whenever the available wind power leads to a flow rate of less than 2.5 m^3/h. The bounded feed flow rate is more elucidated in Fig. 8a. We can see how the feed flow rate is zero at wind power less than 500 kW and saturates at the maximum value when the power exceeds 2,750 kW. This behavior is reflected in the production rate shown in Fig. 8b as it settles at a constant value for P_{wt} > 2,750 kW. This causes a slight reduction in the total production rate which is not very clear in Fig. 7a. However, the calculated LPRP is 16%. Besides the minor loss in total production rate, this type of operation does not completely utilize the available wind power. When the feed flow rate is truncated at maximum value, part of the existing power is not leveraged. The unused power is estimated to be 23%. The unused power when the feed flow rate is set to zero is not counted because it is very small and cannot be utilized to launch the RO anyway. However, this minute power can still be harvested if a lesser number of vessels is employed. Better leverage of the generated power will be discussed in the following.

In summary, the production rate of the wind-RO plant is limited by two factors. The first factor is the available wind power. The second factor is the physical limitation of the RO module when the wind power is either very high or very low. There are two issues related to this situation. There is a chance of wasted wind power because more power could have been used by the RO vessel if the vessel can accept a flow rate higher than 15 m^3/h and/or if a larger number of vessels is used such that the delivered power per vessel is lowered. The second issue is that when the feed flow rate becomes high, the fixed feed pressure becomes relatively small to an extent it operates the RO module below the desired recovery ratio and consequently sacrificing the production rate. On the other hand, when the available wind power is low and the feed pressure is fixed, the feed flow rate decreases below the nominal value. Therefore, the operating pressure becomes relatively high leading to a higher recovery ratio and hence production rate. However, since the recovery ratio is limited by a maximum value of 0.85, which is the largest reported value, the production rate will level off at this threshold even if additional pressure is available. This means some of the

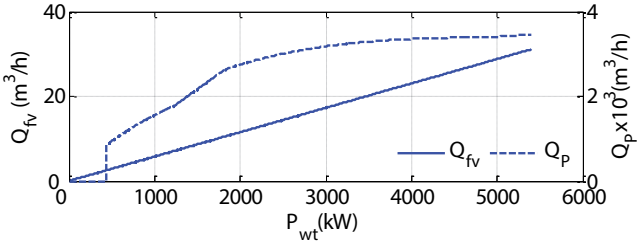

Fig. 6. Feed and production flow rates as a function of the wind power for the results shown in Fig. 5.

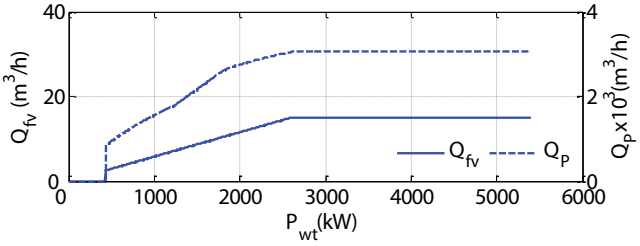

Fig. 8. Feed and production flow rates as a function of the wind power for the results shown in Fig. 7.

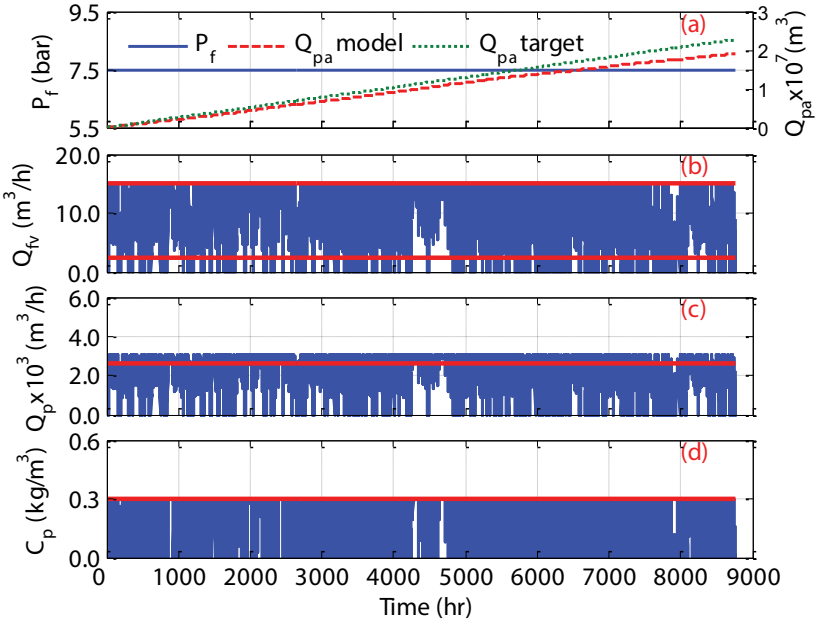

Fig. 7. Simulation of the RO plant at fixed P_f with constraints on the feed flow rate; constant bold line denotes target value for C_p and Q_p and upper and lower limits for Q_f.

applied pressure is wasted. Aside from using batteries or grid electricity, these issues can be counteracted by operational strategies. One way is to use adaptive feed pressure such that the pressure per vessel is optimized during wind power fluctuation. Another way is to use an adaptive number of vessels such that the supplied power is optimally distributed over the utilized vessels. The feasibility of these strategies is assessed in the following sections.

5.2. Adaptive vessel size strategy

By adaptive vessel sizing, we mean adaptive number of active vessels. For example, when excess power beyond that used for operating the pump at maximum capacity is available, it can be harnessed to activate additional vessels beyond the nominal ones. In contrast, when low wind power exists, a smaller number of vessels than the nominal ones can be employed. In due course, the apportioned power per vessel becomes relatively larger providing a sufficient flow rate to operate the vessels. Therefore, enlarging N_v allows accommodating more power into the RO plant while lessening N_v amplifies the supplied power per vessel. The proposed adaptive strategy involves setting the maximum and a minimum number of vessels as follows:

$$N_v^{\max} = \frac{P_w^{\max} \times 3{,}600}{Q_{f\max}\left(\frac{P}{\eta_p}\right)} \tag{10}$$

$$N_v^{\min} = \frac{P_w^{\min} \times 3{,}600}{Q_{f\max}\left(\frac{P}{\eta_p}\right)} \tag{11}$$

Algorithm S2 (Appendix C) is modified such that whenever the generated power leads to a feed flow rate higher than the upper limit, the number of vessels is set equals to the maximum as estimated by Eq. (10). On the other hand, whenever the generated power leads to a feed flow rate lower than the lower limit, the number of vessels is set equals to the minimum as estimated by Eq. (11). This strategy does not imply changing the plant size (number of vessels) on site. Instead, it suggests designing the RO plant using a large pool of vessels. Hence, the adaptive strategy will choose whether to operate the plant fully or partially. The result of the adaptive strategy is depicted in Figs. 9 and 10. Undoubtedly, the performance of the RO plant is enhanced. The feed flow rate is well confined within the limit frame as shown in Fig. 9b. This leads to an enlarged production rate while the water purity is kept within the limit as depicted in Figs. 9c and d. The augmented production rate caused the accumulated production rate to overweigh the accumulated target as illustrated in Fig. 9a with the LPRP is reduced to −0.125. The latter indicates a water abundance of 13% over the required city demand, Fig. 10c shows how the plant operates at different levels of N_v. This led to the smart adaption of the feed flow rate and production rate as depicted in Figs. 10a and b. This adaptation harvested the entire generated wind power, but at the expense of increased capital cost. Note the maximum N_v is 1037 which is around a 108% increase over the nominal case of 500 vessels.

This adaptive strategy can also be tested for different fixed feed pressures. Note the advantage of altering the feed pressure is that it affects $N_v^{\max}$ and $N_v^{\min}$ via Eqs. (10) and (11). Hence it can lead to better leverage of the generated power.

The results are listed in Table 4. Four feed pressure values were examined. For all cases, the adaptive strategy managed to fully harvest the generate power as the unused power is minimal but increases with feed pressure. The

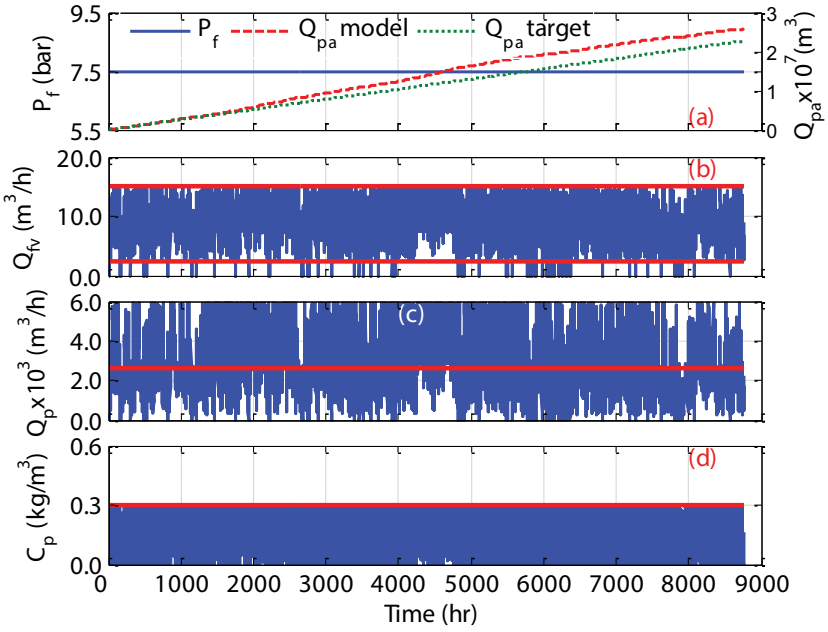

Fig. 9. Simulation of the RO plant at fixed P_f using adaptive vessel size strategy; constant bold line denotes target value for C_p and Q_p and upper and lower limits for Q_f.

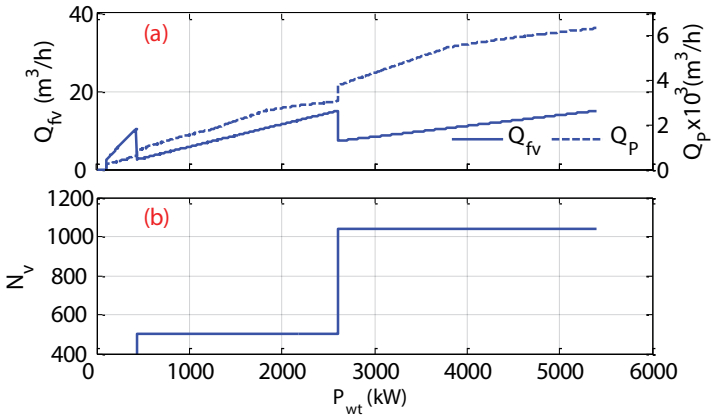

Fig. 10. Feed and production flow rates as a function of the wind power for the results shown in Fig. 9.

Table 4
Comparing adaptive strategy at a different feed pressure

	Adaptive N_v			
P_f (bar)	5	7.5	15	20
Unused power, %	0.028	0.026	0.45	2.26
LPRP	–0.166	–0.136	0.085	0.25
N_v^{min}	500	400	363	272
N_v^{max}	1,555	1,037	518	500

minimal unused power is the smallest wind power that cannot deliver the minimum allowable flow rate. Increasing the feed pressure beyond the nominal value of 7.5 bar is worthless because productivity is lost. At high feed pressure, the feed flow rate is reduced leading to less overall production rate. The additional feed pressure in this case was useful to produce higher water purity. This is however unnecessary since a salinity of 0.5 mg/L is sufficient for potability. At feed pressure of 5 bar, the largest surplus (17%) is reported because more water feed is processed, but at the expense of additional capital investment as the maximum N_v reaches 1555. Obviously, the minimum and maximum number of N_v decrease with feed pressure. This is because the water intake decreases, therefore less N_v is necessary to maintain a reasonable feed flow rate. Thus, the nominal case of 7.5 bar remains the best choice.

5.3. Adaptive feed pressure

An alternative approach is allowing the feed pressure to adapt to changing wind power. Adapting the feed pressure is conceptually equivalent to adapting N_v in the sense of accommodating more energy into the RO plant. In fact, adapting the feed pressure is less expensive because it does not affect the capital investment. Carta et al. [10] proposed a similar approach, where inlet pressure and flow rate are varied. Practically, this can be attained by using automatic control to continuously adjust the feed pressure. In this study, this approach is achieved by simply running algorithm S2 (Appendix C). The outcome of this test is shown in Fig. 11. Clearly, the feed pressure is well adapted to squeeze the feed pressure within the operational envelope without sacrificing the desired water quality in terms of permeate concentration. Because the entire generated power is leveraged, the water production is improved whereas the LPRP reaches −0.03 which corresponds to a 3% surplus. Accordingly, regulating the feed pressure during wind fluctuation can help to improve the RO plant performance and satisfy the city's water hourly demand.

Table 5 compares the performance of the different strategies discussed above which are the fixed fed pressure (FP), fixed feed pressure with active constraints on the feed flow rate (FP_{conf}), fixed feed pressure with adaptive N_v (FR_{adapt}), and variable feed pressure (VP). The comparison is based on three metrics. Note that FP is impractical, but it is included for demonstration purposes. For the case of unused energy, FP_{conf} is the worst as about 23% of the generated power is lost. As far as productivity is concerned, FR_{adapt} is the best with the highest surplus percentage of 13%. The FP_{conf} is inferior as it cannot supply the minimum requirement of water production over the entire year. The power consumption per vessel (P_{wv}) is a crucial measure of the power management for each strategy. For example, FP and VP have the highest power usage because they manage to accommodate more energy per vessel at a fixed total number of vessels. In this case, during high wind power, FP increases the water intake, that is, operating the pump at maximum flow rate while the VP increases the feed pressure. In both cases, the energy consumed per vessel increases. On the other hand, FP-adapt reduces the power intake per vessel by expanding the number of vessels. In conclusion, FP-adapt delivered the best performance in terms of all metrics. Nevertheless, it requires additional capital investment. Moreover, it requires optimal control of feedforward control system that allows for operating different sizes of RO vessels.

For RO plants with a fixed size, that is, N_v is fixed at the nominal case of 500, PV remains the best operation strategy. Hence, we further test this strategy and the adaptive strategy under severe operating conditions. For example, the salinity of the brackish water may vary. Besides, the recovery ratio of the plant may degrade with time due to fouling and scaling. For this reason, we simulate the desalination plant under some degree of uncertainty in the feed salinity and recovery ratio. The disturbance in recovery

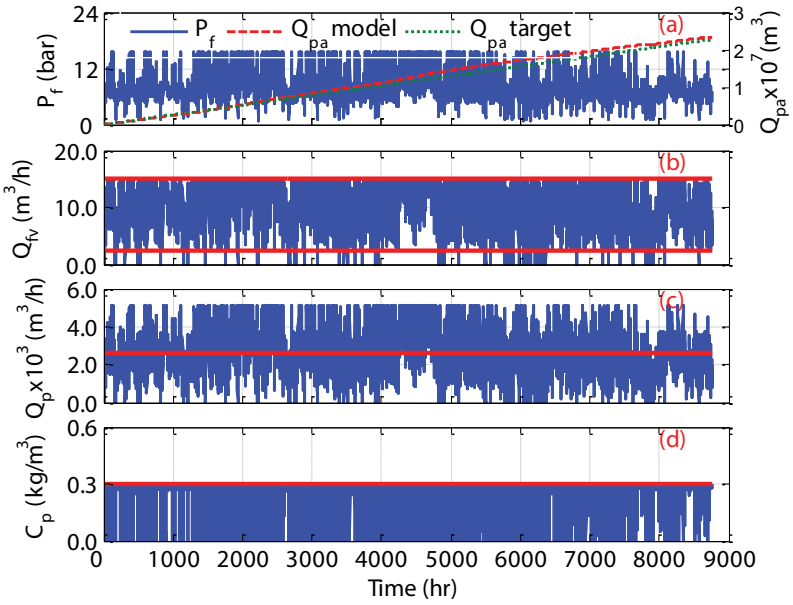

Fig. 11. Simulation of the RO plant using variable P_f; constant bold line denotes target value for C_p and Q_p and upper and lower limits for Q_f.

Table 5
Comparing different operation strategies

	FP	FP_{conf}	FR_{adapt}	VP
Unused power, %	0.00	22.77	0.026	0.00
LPRP	0.13	0.16	−0.13	−0.03
P_{wv} (kW)	4.36	3.64	2.99	4.40

Table 6
RO plant performance under operation uncertainty

	LPRP		
Case	C_f = 1.3 kg/m^3	C_f = 1.7 kg/m^3	C_f = 2 kg/m^3 & R_c = 0.3
Adaptive N_v	0.009	0.183	0.188
Adaptive P_f	0.078	0.189	0.234

ratio is introduced to resemble the effect of fouling. Table 6 summarizes the result of these tests. We can see that as feed salinity increases, the RO plant loses its productivity to an extent that it can no longer provide the water requirements of the city. Note that as feed salinity increases, the osmotic pressure increases degrading the RO production. In this case, higher feed pressure is needed which in turn reduces the water intake. As a result, the overall production rate declines for both strategies. For combined uncertainty in feed salinity and loss in recovery ratio, the RO plant suffers around a 23% shortage in water production for the adaptive pressure strategy. Note also that the adaptive N_v strategy slightly outperforms the adaptive P_f. Although the uncertainty is high, equivalent to a 100% increase in C_f and a 40% reduction in R_c, it highlights the sensitivity level of the RO plant design and operation strategy.

6. Water cost analysis

It is essential to estimate the water production cost for the entire desalination system. The breakdown of the cost components along with the related correlations are listed in Tables 7 and 8. The necessary operating and design parameters of the desalination plant to be used for computing the plant economics are listed in Table 9. Note that computing the capital cost of the storage tanks requires the knowledge of the required volume of water to be stored. According to Table 5, the maximum annual shortage is around 23.4%. This means the plant needs to store at least 23% of the annual production to subsidize the shortages during low wind periods. Hence, we consider the required volume of the storage tank to be 25% of the total annual production. Based on the computed annual operating cost and annualized fixed cost, the specific water cost can be estimated as follows [36]:

$$W_{cost} = \frac{TOC + ACC}{Q_p \times w_{hy}} = 0.45\$ / m^3 \quad (12)$$

When a larger number of vessels is used (in the case of adaptive size), the water cost jumps to 0.52 \$/m^3 for N_v = 1037. This is equivalent to a 16% increase in the specific water cost. Even if the storage tank volume is increased to store the entire annual production, the effect of the tank cost on the water production cost remains negligible. According to Triki et al. [11], the share of the capital cost of the storage tank is less than 1% of the overall capital investment. According to Atab et al. [37], the water cost ranges, depending on the feed salinity and plant capacity, from 0.18 to 7.2 \$/m^3. Hence the estimated water cost in this study fits well with the reported data for general RO plants. Al-Jabr and Ben-Mansour [38] reported a water cost of 0.94 \$/m^3 for a wind-driven RO plant with a daily capacity of 1,000 m^3. Khan et al. [12] surveyed

Table 7
Capital investment cost [9,51]

Component	Correlation		Value ($)
Capital cost for intake pumping and pre-treatment, CC_{IP}	$CC_{IP} = 996(Q_f)^{0.8}$ [52]		11,862,066
Capital cost for the high pressure pumps, CC_{HP}	$\log_{10}C_{hp} = 3.3892 + 0.0536\log_{10}W_{HP} + 0.1538(\log_{10}W_{HP})^2$ [52]		8,931
	$CC_{HP} = N_{HP} \times C_{hp}$ [37]		4,465,458
Capital cost of wind turbine, CC_{WT}	$CC_{WT} = N_{WT} \times P_{wt} \times C_{WT}$ [24]		5,853,600
Capital cost for membranes, CC_{MB}	$CC_{MB} = f_{MB} \cdot C_{MB} \cdot N_{MB}$ [9]		1,480,000
Capital cost of pressure vessels, CC_{PV}	$CC_{PV} = f_{PV} \cdot C_{PV} \cdot N_{PV}$ [9]		500,000
Capital cost of pipes, CC_{pipe}	$CC_{pipe} = 0.4C_E$ [53]		9,664,449
Capital cost of storage tanks, CC_{TK}	$CC_{TK} = 165\left(\frac{V_{TK}}{1000}\right)^{0.57}$	[11]	22,767
Capital cost, CC	$CC = CC_{PV} + CC_{MB} + CC_{pipe} + CC_{HP} + CC_{IP} + CC_{TK}$ [9]		33,848,340
Cost of site development, CC_{site}	$CC_{site} = 0.1CC$ [9]		3,384,834
Direct capital cost, DCC	$DCC = CC + CC_{site}$		37,233,174
Indirect capital cost, ICC	ICC = 0.27DCC [9]		10,052,957
Total capital cost, TCC	TCC = DCC + ICC		47,286,131
Annualized capital cost, ACC	$ACC\left(\frac{\$}{y}\right) = TCC(\$)\frac{i(i+1)^n}{(i+1)^n - 1}$	[9]	4,816,197

Table 8
Annual operating cost [9,10,36,54]

Item	Component	Correlation	Value ($/y)
$OC_{O\&M}$	Annual labor cost	0.01 $/m^3 [54]	204,353
	Annual maintenance cost of potable water	0.01 $/m^3 [54]	204,353
	Annual chemical cost of potable water	0.04 $/m^3 [54]	817,413
	Annual insurance cost	0.05 × TCC [36]	2,362,716
	Total		3,588,836
OC_{MB}	Annual renewal cost for membrane	$C_{MB} \times N_{MB}/n_{LT}$ [9]	296,000
OC_{WT}	Annual maintenance cost for turbines	$C_{Mnt\text{-}WT} \times N_{WT} \times P_{wt}$ [24]	540,000
TOC	Total annual operating cost	$OC_{power} + OC_{OM} + OC_{MB} + OC_{WT}$	4,424,836

several industrial wind-RO plants with capacity ranges from 22 to 7,000 m^3/d where the water cost is found to range from 0.66 to 15.75 $/m^3. Fath et al. [39] recorded water production cost for wind-driven BWRO in the range of 3.9–6.5 $/m^3 for plant capacity ranging from 50 to 2,000 m^3/d. Compared to wind-powered RO plants, our water cost is slightly lower bearing in mind that low feed salinity and very large capacity are used here. For large scale RO plants, water production cost usually becomes lower. For example, Greenlee et al. [40] reported a water cost of 0.55 and 0.53 $/m^3 for a plant capacity of 92,000 and 320,000 m^3/d, respectively. For medium size SWRO plant driven by the grid electricity, Lai et al. [7] reported a water cost range of 0.63 to 3.52 $/m^3. However, the intention is not to compete with the grid-driven desalination plant but rather to alleviate the strain on the local network and protect the environment from the gaseous emission of fossil fuel. Moreover, it is desired to leverage the exiting renewable energy which promotes the vision of diversifying the energy sources.

7. Conclusions

A wind-powered RO desalination plant was designed to supply the hourly water demand for a rural area of Saudi Arabia. The design involved determining the size of the RO plant, that is, the number of needed vessels as well as the operating conditions for these vessels to exactly supply the required water demand. The design also included determining the needed number of wind turbines to supply the necessary power to run the RO plant at the desired conditions. The designed RO-Wind plant was numerically tested under varying hourly wind power without the help of an electricity grid or supporting storage batteries. Three operation strategies were examined and compared. When the plant operates under fixed feed pressure while wind power varies substantially, the desalination plant failed to provide the necessary water demand with a 16% shortage over the entire year. When the plant is modified to allow for the adaptive number of vessels, the plant performance is enhanced

Table 9
Operating and design parameters

Item	Abbreviation	Value
Number of vessels	N_{PV}	500
Number of a high-pressure pump	N_{HP}	500
Number of RO element/vessel	Ne	8
Total number of RO	N_{MB}	4,000
Total number of turbines	N_{WT}	90
Recovery ratio	R_c	0.5
Equipment corrective factor	f_{MB}, f_{PV}	1 [19]
Production rate, m³/h	Q_p	2,592
Feed flow rate, m³/h	Q_f	124,416
Feed flow rate, m³/h	Q_{fmax}	15
Max pump pressure, Pa	P_{max}	8×10^6
Pump efficiency	N_{HP}	0.6
Power of a pump	W_{HP}	55.56
Total pump power, kW	W_{HPt}	27,778
Required wind power, kW	$W_{HPactual}$	1,787
RO surface area, m²	A	37
Membrane unit cost, $/m²	C_{MB}	10 [9]
Vessel unit cost, $	C_{PV}	1,000 [9]
Turbine unit cost, $/kW	C_{WT}	1,084 [24]
Turbine maintenance cost, $/y	$C_{Mnt\text{-}WT}$	100 [24]
Turbine rated power, kW	P_{wt}	60
Interest rate	i	0.08
Plant life, y	n	20
Membrane lifetime, y	n_{LT}	5
Wind turbine lifetime, y	N_{WT}	20
Annual operating hours, h/y	W_{hy}	7,884

such that it provides the required production rate as well as an abundance of 13%. However, this strategy incurs additional capital investment in terms of the number of vessels. Also, it needs a management control system that automatically selects the appropriate RO vessel size in response to the degree of the available wind power. When the plant is operated using variable feed pressure, the plant performance can be improved to deliver the targeted water production in addition to a 3% surplus. The strategy works with the existing plant size but calls for the use of an automatic control system to adapt the feed pressure in the face of varying wind speed. Parametric analysis indicated the failure of the proposed desalination plant to fulfill the desired production rate when a severe disturbance occurs in the feed salinity and/or scale formation on the membrane surface. The economic analysis indicated a water production cost of 0.45 $/m³ for the nominal case which coincides with a similar type and capacity of desalination plants.

Acknowledgment

This study was funded by the National Plan for Science, Technology, and Innovation (MAARIFAH), King Abdulaziz City for Science and Technology, Kingdom of Saudi Arabia, (13-WAT907-02).

Symbols

a — Coefficient for pressure drop correlation
A — Membrane permeability, m/h bar
A_r — Area swept by the rotor blade, m²
A_s — Membrane surface area, m²
B — Membrane solute permeability, m/h
b — Coefficient for viscosity correlation
b_π — Osmotic coefficient, m³ bar/kg
c — Scale parameter
C_f, C_p, C_c — Salt concentration in feed, permeate and brine, kg/m³
C_b, C_m — Average salt concentration and salt concentration at membrane wall, kg/m³
C_{pd} — Desired salt concentration for permeate product, kg/m³
C_F — Capacity factor
D_{AB} — Mass diffusivity, m²/h
d_h — Hydraulic diameter of channel, m
h — Height above the ground level, m
h_g — Height where the wind speed is measured, m
h_{sp} — Height of spacer channel, m
J_w — Water flux, m/h
J_s — Salts mass flux, kg/m² h
k — Shape parameter
k_s — Mass transfer coefficient, m/h
m, m_i — Exponent in Eq. (A2), molality of dissolved salt, ppm
N_{WT} — Number of wind turbines
N_v — Global number of vessels
N — Number of time steps
n_e — Number of RO elements in a vessel
n_l — Number of leaves per RO element
P_w — Average wind power, W
P_{wv} — Wind power per vessel, W
P_{wt} — Total supplied power, kW
P_{wmax} — Wind power corresponding to maximum flow rate, W
P_f, P_b — Feed, permeate, and brine pressure, bar
P_{drop} — Pressure drop, bar
P_r — Rated power, kW
PR — Productivity ratio
P_{os} — Osmotic pressure based on feed salinity, bar
Q_{cv} — Brine volumetric flow rate per vessel, m³/h
Q_b — Mean volumetric flow rate through membrane channel, m³/h
Q_{fv}, Q_{pv} — Feed and permeate flow rate per vessel, m³/h
Q_p — Water demand of the city, m³/h
Q_{pa} — Accumulative production, m³
Q_{fmax} — Maximum allowable feed flow rate, m³/h
Q_w — Production rate based on mass flux, m³/h
Q_{wt} — Total plant production rate, m³/h
R_c — Recovery ratio, %
Re — Reynolds number
SEC — Specific energy consumption, kWh/m³
Sc — Schmidt number
Sh — Sherwood number
t_i — Time at step i
u_c — Cut-in wind speed, m/s
u_f — Cut-out wind speed, m/s
u_r — Rated wind speed, m/s

u — Velocity of water in feed channel, m/h
u_w — Wind velocity, m/s
W — Width of the membrane, m
α — Power-law exponent
ρ — Air density, kg/m^3
ε — Termination factor also void fraction
η_p — Pump efficiency
π — Osmotic pressure, bar
λ — Coefficient for pressure drop correlation
ν — Kinemtic viscosity, m^2/s
μ — Viscosity, Pa s

References

[1] G.Th. Vlachos, J.K. Kaldellis, Application of gas-turbine exhaust gases for brackish water desalination: a techno-economic evaluation, Appl. Therm. Eng., 24 (2004) 2487–2500.
[2] K.K.J.K. Kaldellis, J. Garofallakis, K. Kavadias, Renewable Energy Solution for Clean Water Production in the Aegean Archipelago Islands, Mediterranean Conference on Policies and Strategies for Desalination and Renewable Energies, Santorini Island, Greece, 2000.
[3] R. Dashtpour, S.N. Al-Zubaidy, Energy efficient reverse osmosis desalination process, Int. J. Environ. Sci. Dev., 3 (2012) 339–345.
[4] C. Charcosset, A review of membrane processes and renewable energies for desalination, Desalination, 245 (2009) 214–231.
[5] M.M. Salah, A.G. Abo-khalil, R. Praveen, Wind speed characteristics and energy potential for selected sites in Saudi Arabia, J. King Saud Univ.-Eng. Sci., 33 (2019) 119–128.
[6] E. Ali, A. Ajbar, M. Boumaza, Performance assessment of a wind driven membrane desalination unit in Saudi Arabia, J. Eng. Res., 5 (2017) 43–67.
[7] W.Y. Lai, Q.F. Ma, H. Lu, S.J. Weng, J.Q. Fan, H.X. Fang, Effects of wind intermittence and fluctuation on reverse osmosis desalination process and solution strategies, Desalination, 395 (2016) 17–27.
[8] J. Marriott, E. Sørensen, A general approach to modelling membrane modules, Chem. Eng. Sci., 58 (2003) 4975–4990.
[9] F. Vince, F. Marechal, E. Aoustin, P. Bréant, Multi-objective optimization of RO desalination plants, Desalination, 222 (2008) 96–118.
[10] J.A. Carta, J. González, P. Cabrera, V.J. Subiela, Preliminary experimental analysis of a small-scale prototype SWRO desalination plant, designed for continuous adjustment of its energy consumption to the widely varying power generated by a stand-alone wind turbine, Appl. Energy, 137 (2015) 222–239.
[11] Z. Triki, M.N. Bouaziz, M. Boumaza, Techno-economic feasibility of wind-powered reverse osmosis brackish water desalination systems in southern Algeria, Desal. Water Treat., 52 (2014) 1745–1760.
[12] M.A.M. Khan, S. Rehman, F.A. Al-Sulaiman, A hybrid renewable energy system as a potential energy source for water desalination using reverse osmosis: a review, Renewable Sustainable Energy Rev., 97 (2018) 456–477.
[13] M.S. Miranda, D. Infield, A wind-powered seawater reverse-osmosis system without batteries, Desalination, 153 (2003) 9–16.
[14] I. de la Nuez Pestana, F.J.G. Latorre, C.A. Espinoza, A.G. Gotor, Optimization of RO desalination systems powered by renewable energies. Part I: wind energy, Desalination, 160 (2004) 293–299.
[15] B.S. Richards, G.L. Park, T. Pietzsch, A.I. Schäfer, Renewable energy powered membrane technology: brackish water desalination system operated using real wind fluctuations and energy buffering, J. Membr. Sci., 468 (2014) 224–232.
[16] O. Charrouf, A. Betka, S. Abdeddaim, A. Ghamri, Artificial Neural Network power manager for hybrid PV-wind desalination system, Math. Comput. Simul., 167 (2020) 443–460.
[17] W.X. Peng, A. Maleki, M.A. Rosen, P. Azarikhah, Optimization of a hybrid system for solar-wind-based water desalination by reverse osmosis: comparison of approaches, Desalination, 442 (2018) 16–31.
[18] E.Sh. Mohamed, G. Papadakis, Design, simulation and economic analysis of a stand-alone reverse osmosis desalination unit powered by wind turbines and photovoltaics, Desalination, 164 (2004) 87–97.
[19] W. Khiari, M. Turki, J. Belhadj, Power control strategy for PV/Wind reverse osmosis desalination without battery, Control Eng. Pract., 89 (2019) 169–179.
[20] G.L. Park, A.I. Schäfer, B.S. Richards, Renewable energy powered membrane technology: the effect of wind speed fluctuations on the performance of a wind-powered membrane system for brackish water desalination, J. Membr. Sci., 370 (2011) 34–44.
[21] P. Cabrera, J.A. Carta, J. González, G. Melián, Wind-driven SWRO desalination prototype with and without batteries: a performance simulation using machine learning models, Desalination, 435 (2018) 77–96.
[22] N. Al-Bastaki, A. Abbas, Permeate recycle to improve the performance of a spiral-wound RO plant, Desalination, 158 (2003) 119–126.
[23] A.A. Al-Naeem, Monitoring of groundwater salinity for water resources management in irrigated areas of Al-Jouf region, Saudi Arabia, Res. J. Environ. Sci., 9 (2015) 256–269.
[24] A. Maleki, F. Pourfayaz, M.A. Rosen, A novel framework for optimal design of hybrid renewable energy-based autonomous energy systems: a case study for Namin, Iran, Energy, 98 (2016) 168–180.
[25] J.S. Kim, J. Chen, H.E. Garcia, Modeling, control, and dynamic performance analysis of a reverse osmosis desalination plant integrated within hybrid energy systems, Energy, 112 (2016) 52–66.
[26] G. Srivathsan, Modeling of Fluid Flow in Spiral Wound Reverse Osmosis Membranes, Thesis or Dissertation, Retrieved from the University of Minnesota Digital Conservancy, 2013. Available at: https://hdl.handle.net/11299/158160.
[27] https://membranes.com/docs/trc/Dsgn_Lmt.pdf
[28] https://www.stats.gov.sa/ar/3123
[29] A.S. Stillwell, M.E. Webber, Predicting the specific energy consumption of reverse osmosis desalination, Water, 8 (2016) 601, doi: 10.3390/w8120601.
[30] A.J. Karabelas, C.P. Koutsou, M. Kostoglou, D.C. Sioutopoulos, Analysis of specific energy consumption in reverse osmosis desalination processes, Desalination, 431 (2018) 15–21.
[31] M.A.M. Ramli, S. Twaha, Z. Al-Hamouz, Analyzing the potential and progress of distributed generation applications in Saudi Arabia: the case of solar and wind resources, Renewable Sustainable Energy Rev., 70 (2017) 287–297.
[32] A.M. Eltamaly, A.A. Al-Shamma'a, Optimal configuration for isolated hybrid renewable energy systems, J. Renewable Sustainable Energy, 8 (2016) 045502, doi: 10.1063/1.4960407.
[33] A.M. Eltamaly, Pairing between sites and wind turbines for Saudi Arabia Sites, Arabian J. Sci. Eng., 39 (2014) 6225–6233.
[34] M.J.M. Stevens, P.T. Smulders, The estimation of the parameters of the Weibull wind speed distribution for wind energy utilization purposes, Wind Eng., 3 (1979) 132–145.
[35] U. Bawah, K.E. Addoweesh, A.M. Eltamaly, Economic modeling of site-specific optimum wind turbine for electrification studies, Adv. Mater. Res., 347–353 (2011) 1973–1986.
[36] M.G. Marcovecchio, P.A. Aguirre, N.J. Scenna, Global optimal design of reverse osmosis networks for seawater desalination: modeling and algorithm, Desalination, 184 (2005) 259–271.
[37] M.S. Atab, A.J. Smallbone, A.P. Roskilly, An operational and economic study of a reverse osmosis desalination system for potable water and land irrigation, Desalination, 397 (2016) 174–184.
[38] A.H. Al-Jabr, R. Ben-Mansour, Optimum Selection of Renewable Energy Powered Desalination Systems, Multidisciplinary Digital Publishing Institute Proceedings, 2018, pp. 612, doi: 10.3390/proceedings2110612.
[39] H. Fath, A. Sadik, T. Mezher, Present and future trend in the production and energy consumption of desalinated water in GCC countries, Int. J. Therm. Environ. Eng., 5 (2013) 155–165.

[40] L.F. Greenlee, D.F. Lawler, B.D. Freeman, B. Marrot, P. Moulin, Reverse osmosis desalination: water sources, technology, and today's challenges, Water Res., 43 (2009) 2317–2348.
[41] https://en.wind-turbine-models.com/turbines/812-ades-ades-60
[42] https://en.wind-turbine-models.com/turbines/1682-hummer-h25.0-100kw
[43] http://www.neicjapan.com/smallwindmill/Aeolos-H%20100kW%20Brochure.pdf
[44] https://www.norvento.com/en/for-large-companies/
[45] https://en.wind-turbine-models.com/turbines/859-aircon-10s
[46] https://en.wind-turbine-models.com/turbines/1829-aeolia-windtech-d2cf-200
[47] https://en.wind-turbine-models.com/turbines/956-air-19-100
[48] https://en.wind-turbine-models.com/turbines/144-allgaier-stgw-34
[49] https://en.wind-turbine-models.com/turbines/1026-ae-italia-stoma-st-k60-d21
[50] https://en.wind-turbine-models.com/turbines/1876-dencon-tornado-200-26
[51] Y.-Y. Lu, Y.-D. Hu, X.-L. Zhang, L.-Y. Wu, Q.-Z. Liu, Optimum design of reverse osmosis system under different feed concentration and product specification, J. Membr.Sci., 287 (2007) 219–229.
[52] A. Malek, M.N.A. Hawlader, J.C. Ho, Design and economics of RO seawater desalination, Desalination, 105 (1996) 245–261.
[53] M. D'Adda, Fixed-capital cost estimating, Catal. Today, 34 (1997) 457–467.
[54] Y. Dreizin, Ashkelon seawater desalination project? off-taker? self costs, supplied water costs, total costs and benefits, Desalination, 190 (2006) 104–116.
[55] T. Sherwood, P. Brian, R. Fisher, Desalination by reverse osmosis, Ind. Eng. Chem. Fundam., 6 (1967) 2–12.
[56] J. Schultz, Synthetic Membranes: Science, Engineering and Applications, P.M. Bungay, H.K. Lonsdale, M.N. de Pinho, Eds., D. Reidel Publishing Co., Dordrecht, 1986, pp. 523–566.
[57] A. Da Costa, A. Fane, D. Wiley, Spacer characterization and pressure drop modelling in spacer-filled channels for ultrafiltration, J. Membr. Sci., 87 (1994) 79–98.
[58] Sourirajan, Reverse Osmosis, Logos Press Ltd., London, UK, 1970.

Appendix A

For a single reverse osmosis (RO) module, the feed flow rate per vessel can be calculated from [11]:

$$Q_{\text{fv}} = \frac{3{,}600 \times P_w}{P_f \times 1 \times 10^5 \eta_p^{-1}} \tag{A1}$$

where P_w is the pump power, η_p is the pump efficiency and P_f is the applied pressure. For a given recovery ratio (R_c), the purified water production (permeate) per vessel (Q_{pv}) is determined as follows:

$$Q_{\text{pv}} = Q_{\text{fv}} R_c \tag{A2}$$

Applying solvent and solute mass balance around the RO unit, yields:

$$Q_{\text{fv}} = Q_{\text{pv}} + Q_{\text{cv}} \tag{A3}$$

$$Q_{\text{fv}} C_f = Q_{\text{pv}} C_p + Q_{\text{cv}} C_c \tag{A4}$$

In Eq. (A3) and (A4) C_f, C_p, C_c are the salinity of the feed, permeate and concentrated brine. Q_{cv} in the brine flow rate. The flow rate of bulk solution (Q_b) and its salinity (C_b) are approximated by:

$$Q_b = \frac{Q_{\text{fv}} + Q_{\text{cv}}}{2} \tag{A5}$$

$$C_b = \frac{C_f + C_c}{2} \tag{A6}$$

Given the membrane permeability coefficient (A), the water volumetric flux, J_w, is given by [9]:

$$J_w = A\left(\Delta P - \Delta\pi\right) \tag{A7}$$

where the following correlation for transmembrane pressure drop (ΔP) [9] is used:

$$\Delta P = P_f - P_b - \frac{P_{\text{drop}}}{2} \tag{A8}$$

$$\Delta\pi = b_\pi \left(C_m - C_p\right) \tag{A9}$$

where P_b is the outlet brine pressure, C_m is the salinity at the membrane interface, and P_{drop} is the pressure drop along the membrane length. The osmotic coefficient, b_π, is defined as follows:

$$b_\pi = \frac{\pi}{C_b} \tag{A10}$$

The osmotic pressure, π, is computed using the following expression [11]:

$$\pi = 1.12 \times T \sum \bar{m}_i \tag{A11}$$

where $\sum \bar{m}_i$ as the sum of all modalities of dissolved ions (ppm) and T is the bulk temperature.

The pressure drop, P_{drop}, can be estimated using the following correlation [9]:

$$P_{\text{drop}} = 9.5 \times 10^8 \left(\frac{Q_f + Q_c}{2 \times 3{,}600}\right)^{1.7} \tag{A12}$$

The mass flux, J_s, of the solute in terms of its permeability coefficient (B) is defined as follows:

$$J_s = B\left(C_m - C_p\right) \tag{A13}$$

In the presence of concentration polarization, which is typical for RO processes, the flux, J_w, at steady state, is given in terms of the mass transfer coefficient (k_s) by [55]:

$$J_w = k_s \ln \frac{C_m - C_p}{C_b - C_p} \tag{A14}$$

The solute flux and the solvent flux are related to each other's via:

$$J_s = J_w C_p \tag{A15}$$

The combination of Eqs. (A10)–(A12) and the elimination of C_m leads to the following relationship for the flux [56]:

$$J_w = A\left[\Delta P - b_\pi\left(\frac{BC_b\exp\left(J_w/k_s\right)}{J_w + B\exp\left(J_w/k_s\right)}\right)\exp\left(J_w/k_s\right)\right] \quad \text{(A16)}$$

$$C_p = \frac{BC_b}{B + J_w\exp\left(J_w/k_s\right)} \quad \text{(A17)}$$

The nonlinear algebraic equations (A1)–(A17) can be solved numerically and simultaneously to determine the permeate concentration, C_p, and the permeate production rate, Q_w. The latter defines the distillate production based on the mass flux as follows:

$$Q_w = J_w A_s n_e n_l \quad \text{(A18)}$$

where A_s is the surface area of the membrane, n_e is the number of RO elements per vessel, and n_l is the number of leaves per RO element. Perforated baffles are used in spiral-wound membrane modules to enhance mass transfer. Hence, the mass transfer coefficient, k_s which is required in Eqs. (A16) and (A17) can be estimated as follows [57]:

$$S = 0.065\,\mathrm{Re}^{0.865}\,\mathrm{Sc}^{0.25} \quad \text{(A19)}$$

where

$$\mathrm{Sh} = \frac{k_s}{D_{\mathrm{AB}}};\ \mathrm{Re} = \frac{d_h u}{\mu};\ \mathrm{Sc} = \frac{v}{D_{\mathrm{AB}}} \quad \text{(A20)}$$

where μ, ν, D_{AB} are the viscosity, kinematic viscosity and diffusivity of water. d_h is the hydraulic diameter. The velocity in the feed channel (u) that contains baffle is given by:

$$u = \frac{Q_b}{wh_{\mathrm{sp}}\varepsilon} \quad \text{(A21)}$$

d_h, h_{sp}, and ε is the baffle parameters. The kinematic viscosity, ν, for brackish water can be calculated through the following correlation [58]:

$$\nu = 0.0032 + 3.0\times10^{-6}C_b + 4.0\times10^{-9}C_b^2 \quad \text{(A22)}$$

The value of diffusivity, D_{AB}, is given as 5.5×10^{-6} m²/h [11].

The RO process performance is measured via two indices. The recovery ratio is defined as follows:

$$R_c = \frac{Q_w}{Q_{\mathrm{fv}}} \quad \text{(A23)}$$

The energy required per 1 m³ of freshwater is known as the specific energy consumption and expressed as follows [20]:

$$\mathrm{SEC} = \frac{Q_{\mathrm{fv}}P_f\eta_p^{-1}}{Q_{\mathrm{pv}}} \quad \text{(A24)}$$

Usually, the permeate salinity must meet potability conditions, that is, salt concentration in the permeates must be smaller than a desired specific value, C_{pd}:

$$C_p \le C_{\mathrm{pd}} \quad \text{(A25)}$$

Appendix B

The algorithm (S1) for the backward mode is:

1. Define all process parameters and operating conditions such as C_f, Q_p, N_v, and R_c'
2. Set $Q_{\mathrm{pv}} = Q_p/N_v$
3. Compute Q_{fv} using Eq. (A2)
4. Solve the following optimization problem:

$$\min_{P_f, C_p^o, C_m^o} \varphi = \left(R_c - R_c'\right)^2 \quad \text{(B1)}$$

Subject to:

$$C_p \le C_{\mathrm{pd}} \quad \text{(B2)}$$

$$C_p - C_p^o = 0 \quad \text{(B3)}$$

$$C_m - C_m^0 = 0 \quad \text{(B4)}$$

$$\pi C_f < P_f \le 40 \quad \text{(B5)}$$

5. Compute the power per vessel using Eq. (A1)
6. Compute SEC using Eq. (A24)

Appendix C

The algorithm (S2) for the forward mode for fixed feed pressure is:

1. Define all process parameters and operating conditions such as C_f, P_{wt}, N_v, and R_c'
2. Set $P_w = P_{\mathrm{wt}}/N_v$
3. Solve the optimization problem defined by Eqs. (B1)–(B5) in addition to the following constraint:

$$Q_{f\min} \le Q_{\mathrm{fv}} \le Q_{f\max} \quad \text{(C1)}$$

Note, the last constraint is imposed to ensure the obtained result respect the safe operation window.

Appendix D

The algorithm (S3) for the forward mode for variable feed pressure:

1. Define all process parameters and operating conditions such as C_f, P_{wt}, P_f, N_v, and R_c'
2. Set $P_w = P_{\mathrm{wt}}/N_v$
3. Compute Q_{fv} using Eq. (A1)
4. Assume initial values for $C_p = C_p^o$ & $C_m = C_m^o$
5. Compute Eqs. (A3)–(A17)
6. If $C_p - C_p^o < \varepsilon$ & $C_m - C_m^o < \varepsilon$, where C_m and C_p are computed from Eqs. (A14) and (A17), respectively, proceed to step 7, otherwise set $C_p^o = C_p$ & $C_m^o = C_m$ go back to step 5
7. Compute Q_w and R_c